# Indonesia coverage simulation of SAR satellite at near-equatorial orbit

**Harry Septanto, Satriya Utama, Robertus Heru Triharjanto and Suhermanto**

Satellite Technology Center, National Institute of Aeronautics and Space (LAPAN), Indonesia

E-mail: harry.septanto@lapan.go.id

**Abstract**. Properties of SAR (Synthetic Aperture Radar) that able to penetrate the cloud and does not depend on the sunlight are a number of advantages when utilized for monitoring tropical region like the IMC (Indonesian Maritime Continent). Moreover, since having areas along equatorial belt, the IMC is at a shortcoming from perspective of highly inclined LEO (Low Earth Orbit) satellite. It would result shorter and infrequent pass times when compared with a near-equatorial LEO satellite whose low inclination. This paper reports on the investigation of a near-equatorial LEO SAR satellite coverage property through simulations. The simulations is run in nine scenarios of orbit parameter that consist of combinations of attitude {500 km, 600 km, 700 km} and inclination {80, 90, 100}. The target area is defined as 50 km x 50 km around Jakarta. Meanwhile, the SAR sensor simulation is run with swath width of 40 km, incidence angle around $25^0$-$29^0$ and Stripmap mode. Minimum, Maximum and Mean Access Revisit of the target for each scenarios are resulted.

## 1. Introduction

SAR (synthetic aperture radar) is a type of radar system installed on a moving platform, such as UAV (unmanned aerial vehicle), aircraft or satellite. The objective of the radar is to acquire images of phenomena over the surface of the Earth. Earth observation capabilities provided by a SAR that is carried by a satellite as the payload have been enthused by researchers for years. Unlike optical camera payload that depend on Sun illumination, SAR payload can be operated in all-weather and day-night time. Therefore, it is very valueable for the monitoring of areas with high cloud coverage such as Indonesia. Images acquired from SAR satellites are employed over a wide range of applications including to classify tropical natural forest and plantation and to track plantation dynamics [1], to detect ships [2] and to monitor small land deformation that indicates environmental degradation at urban area [3][4]. In addition, another applications are to generate actual oil spill distribution maps for the Northern Caspian and the Eastern Black Sea [5], to study accurateness burned area mapping in relating to the soil and snag moisture [6], to quantify the amount of snow mass [7], for tomographic analysis of forest volumes [8], to classify coastal zone terrains [9], to generate to identify rice fields in Vietnam [10], to retrieve agricultural crop [11], to monitor glacier surface motion [12], to get better understanding and quantification of surface roughness of sea ice [13], to provide flood mapping in urban areas [14], to name a few.

SAR satellites have been operating since 1978 with the launch of US SAR satellite SEASAT. At the moment, many nations operate SAR satellite system such as Radarsat (Canada), ALOS (Japan),

TerraSAR-X (Germany) and many others. X, C, and L-band are the most popular choice for the radar frequency and the resolution are varied from 3 m, for vehicle class observation, to 100 m for large area observation.

Most of satellites including the satellites stated above are at highly inclined LEO (Low Earth Orbit). Since having areas along equatorial belt, the IMC (Indonesian Maritime Continent) is at a shortcoming from perspective of highly inclined LEO (Low Earth Orbit) satellite. It would result shorter and infrequent pass times when compared with a near-equatorial LEO satellite whose low inclination. Meanwhile, near-equatorial orbit is a new trend in Earth observation satellites recent years, since more countries in equatorial belts in owning Earth observation satellites. In July 2009, Malaysia launched a near-equatorial orbit satellite called Razaksat-1 which has 400 kg mass. The satellite has multispectral imager with 5 m resolution and panchromatic camera with 2.5 m resolution. It is launched to 685 km orbit with 9º inclination. From such orbit the camera was operated from Malaysia six passes per day, until its radio failed in one year after launched [15]. In September 2015, a 78 kg near-equatorial orbit satellite is launched by Indonesia that is called LAPAN-A2/ LAPAN-ORARI satellite [16]. The satellite is launched to 638 km orbit with 6º inclination. It passes Indonesia nine times per day with brings multi-mission including 24 hours AIS (automated identification system) receiver run to track vessels and ships. In December 2015, Singapore launched a near- equatorial orbit satellite which has 500 kg mass to 550 km orbit with $15^0$ inclination. The satellite carries panchromatic camera with 1 m resolution and has mean revisit time of 12-16 hours [17].

Currently, there is none of SAR satellite operates at near-equatorial LEO even though the satellite might provide many advantages to nations that have areas along equatorial belt. Hence, studies on the design of the SAR satellite that operates at near-equatorial LEO is challenging, besides would be valuable, especially in the context of the IMC. This paper reports on the investigation of a coverage properties aspect of a near-equatorial LEO SAR satellite.

## 2. Simulation Setup

A commercial simulation software called STK (System Tool Kit) Pro version 11 from AGI (Analytical Graphics, Inc.) [18] is utilized to run the simulation. Orbit parameters of the satellite used in the simulation is presented in Table 1. In addition, the simulation implements J4 orbit perturbation propagator model which considers the Earth oblateness effects. It is well-known that the Earth oblateness effects is the major orbit perturbation effect for most SAR satellites [20].

**Table 1**. Satellite's orbit parameters

| | |
|---|---|
| **Orbit's Shape** | Circular |
| **Argument of Perigee** | $90^0$ |
| **RAAN (Right Ascension of Ascending Node)** | $0^0$ |

There are nine scenarios that accommodate combination values between altitude and inclination as shown in Table 2. Meanwhile, for all of scenarios, the SAR system is run such that it has about $25^0$-$29^0$ incidence angle and about 40 km swath width. The SAR sensor model used in the simulation is Complex Conic type. This sensor type selection follows the consideration in [19].

Inner (outer) incidence angle of the SAR system, as depicted in Figure 1, is represented by the Inner (Outer) Half Angle parameter of the sensor model. Equation (1) represents the mathematical relation between the incidence angle, $\theta$, and the Half Angle, $\alpha$, [19].

$$\alpha = \sin^{-1}\left(\frac{R_E}{R_E + h}\sin(\theta)\right) \tag{1}$$

where $R_E$ is radius of the Earth and $h$ is the satellite's altitude.

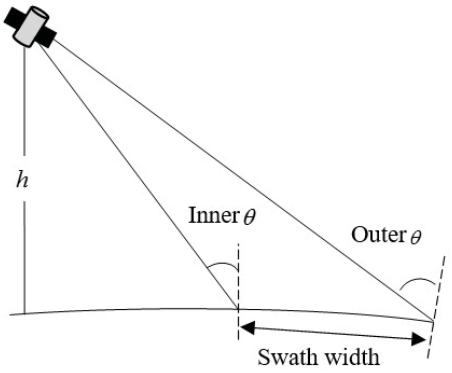


**Figure 1.** SAR system parameters

**Table 2**. Combinations of altitude and inclination

| Scenario No. | Altitude (km) | Inclination ($^0$) |
|---|---|---|
| 1 | 500 | 8 |
| 2 | 600 | 8 |
| 3 | 700 | 8 |
| 4 | 500 | 9 |
| 5 | 600 | 9 |
| 6 | 700 | 9 |
| 7 | 500 | 10 |
| 8 | 600 | 10 |
| 9 | 700 | 10 |

The radar projection on ground (sensor footprint) is formed by defining an inner incidence angle and tuning the outer incidence angle parameter as well as the Minimum and Maximum Clock Angle parameters of the Complex Conic sensor model. The inner incidence angle is defined by $25^0$ for all scenarios. It yields a set of outer incidence angle that varies from $28^0$ to $29^0$. For each scenario, these values are converted to Inner and Outer Half Angle through equation (1) as appeared in Table 3. Moreover, for each scenario, the Minimum Clock Angle is $89.9^0$ and the Maximum Clock Angle is $90.1^0$ to represent a side-looking radar with a narrow beam width. For each scenario, the SAR system is assumed run Stripmap mode with the defined fixed parameters.

**Table 3**. Incidence Angles and sensor model's Half Angle equivalent value

| Scenario No. | Incidence Angle ($^0$) | | Half Angle ($^0$) | |
|---|---|---|---|---|
| | Inner | Outer | Inner | Outer |
| 1 | 25 | 29 | 23.0706 | 26.7135 |
| 2 | 25 | 28.5 | 22.7209 | 25.8546 |
| 3 | 25 | 28 | 22.3821 | 25.0239 |
| 4 | 25 | 29 | 23.0706 | 26.7135 |

| Scenario No. | Incidence Angle ($^0$) | | Half Angle ($^0$) | |
|---|---|---|---|---|
| | Inner | Outer | Inner | Outer |
| 5 | 25 | 28.5 | 22.7209 | 25.8546 |
| 6 | 25 | 28 | 22.3821 | 25.0239 |
| 7 | 25 | 29 | 23.0706 | 26.7135 |
| 8 | 25 | 28.5 | 22.7209 | 25.8546 |
| 9 | 25 | 28 | 22.3821 | 25.0239 |

The target area is defined as 50 km to 50 km north side of Jakarta, Indonesia. This area is depicted in Figure 2.

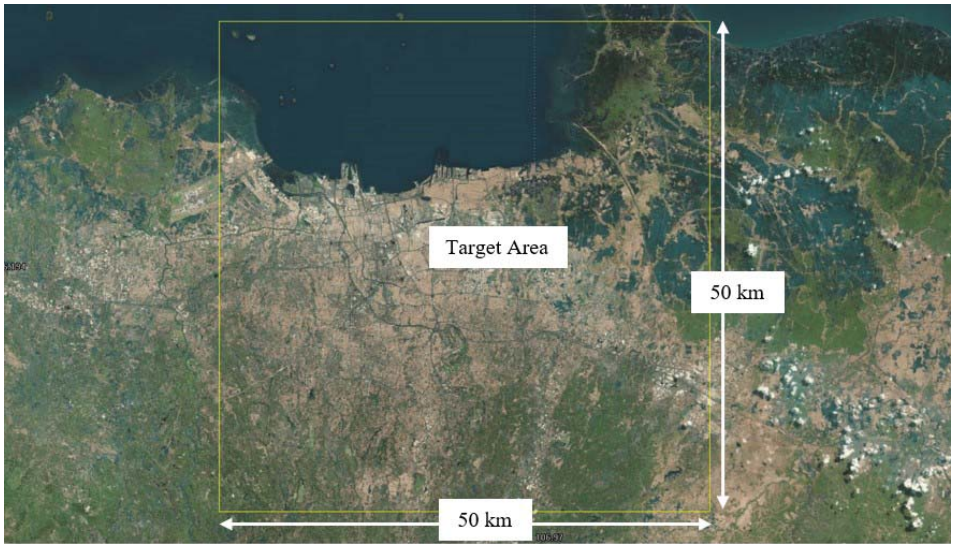


**Figure 2.** Target area

## 3. Results and Discussion

The following terminologies that represents coverage properties are necessary to be defined to further discuss the simulation result:

- *Access to Target* occurs when there is an intersection between the sensor footprint and the target.
- *Start Time of Access to Target* is a time when the Access to Target began.
- *Access Revisit* is the time elapsed between two consecutive start times of Access to Target.
- *Mean Access Revisit* is average of access revisit in one year.

**Table 4**. Coverage properties in 1 year

| | Minimum | | Maximum | |
|---|---|---|---|---|
| **Total Access to Target** | 145 times | Scenario 9 | 201 times | Scenario 1 |
| **Access Revisit** | 8.4 hours | Scenario 4/ 7 | 15.1 days | Scenario 9 |
| **Mean Access Revisit** | 1.8 days | Scenario 9 | 2.5 days | Scenario 1 |

Data presented in Table 4 describes a brief result obtained from the simulation run. These coverage properties are obtained for 1 year simulation time. The Access Revisit and Mean Access Revisit data in Table 4 are roundness values. The orbit's parameters of Scenario 1 yields the maximum times of Access to Target and Mean Access Revisit, i.e. 201 times and 2.5 days, respectively. Meanwhile, simulation results using Scenario 9 presents the longest Access Revisit, i.e. 15.1 days. In addition, simulation results of each scenario are presented in Figure 3, Figure 4 and Figure 5.

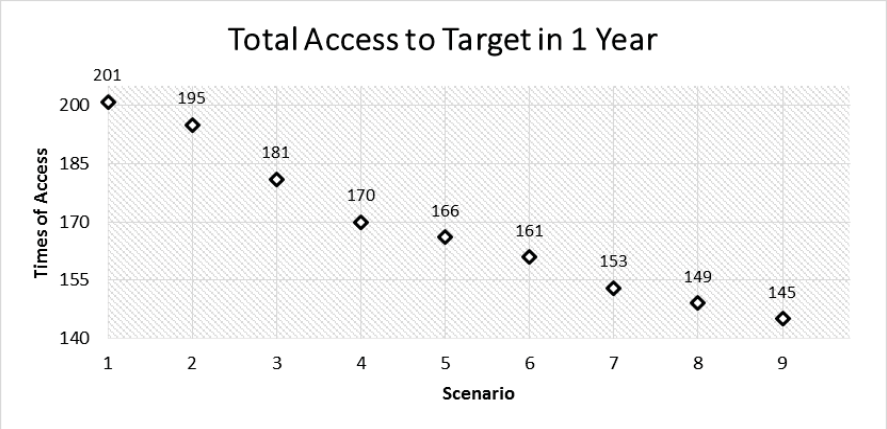


**Figure 3.** Total Access to Target in 1 year of each scenario

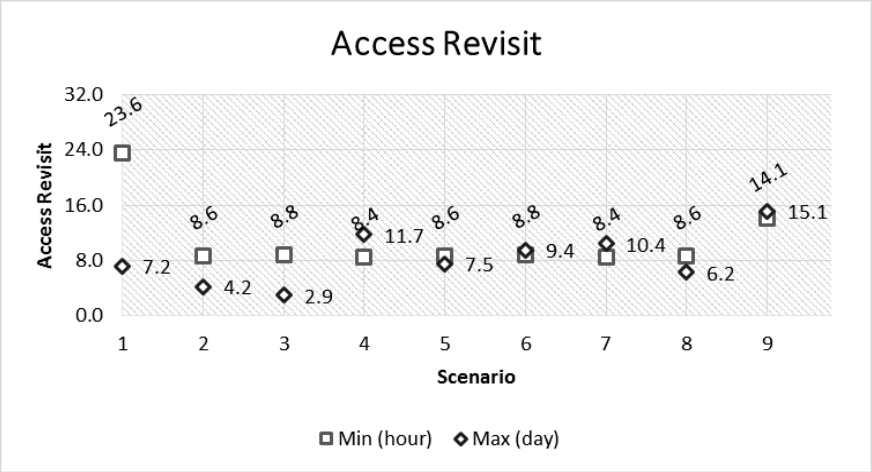


**Figure 4.** Minimum and maximum Access Revisit of each scenario

Figure 3 describes that, for a same inclination setting, total Access to Target decreases when altitude increases. This trend also apprear in Figure 5 that for a same inclination setting, Mean Access Revisit decreases when altitude increases. Meanwhile, differs from these figures, Figure 4 shows fluctuate values. An interest finding is that the orbit parameters of Scenario 2-8 yield similar values of the minimum Access Revisit.

In polar or near-polar orbit, Revisit Time is a terminology that is often used to represent a coverage property, i.e. the time elapsed between observations of the exact same location on Earth. Its value represents temporal resolution of the SAR-based remote sensing system which is an important consideration in many applications [22]. However, a near-equatorial orbit case produces different

behavior of path than polar or near-polar orbit case that implies in difficulty of Revisit Time calculation. Instead, especially in this paper, the temporal resolution is represented by (Mean) Access Revisit. Simulation results show that the near-equatorial SAR satellite has higher temporal resolution (Mean Access Revisit), i.e. about two days, than a polar or near-polar orbit SAR satellite that has more than a week of Revisit Time, e.g. TerraSAR-X has 11 days [21].

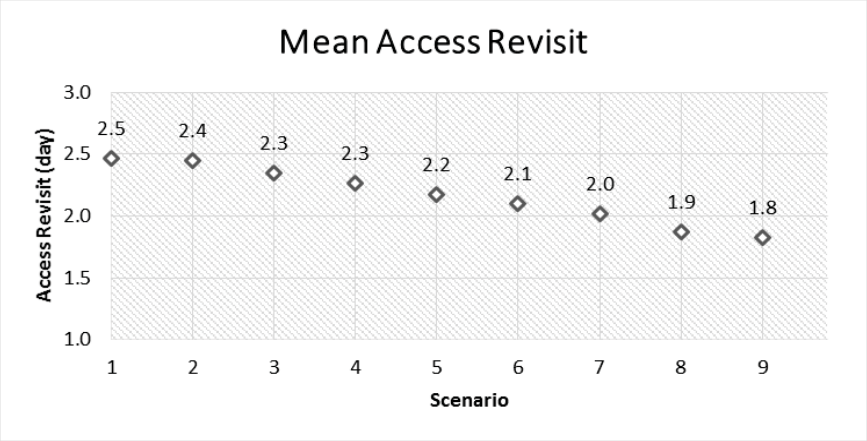


**Figure 5.** Mean Access Revisit of each scenario

## 4. Concluding Remarks

Study on SAR-based remote sensing satellite at a near-equatorial orbit is challenging. Through simulation, coverage properties with respect to a 50 km x 50 km target area at north side of Jakarta, Indonesia, are resulted. Each scenario (Mean) Access Revisit that is considered as the temporal resolution of the near-equatorial orbit satellite is presented.

These research results can be further developed with respect to entire area of Indonesia Maritime Contingent. Moreover, a more realistic SAR system model and another SAR modes, i.e. spotlight and scanSAR, are challenging to be implemented in the simulation to obtain more comprehensive coverage properties analysis. Eventually, these research results may become an important part in designing a SAR-based remote sensing satellite at a near-equatorial orbit.

## Acknowledgement

This work is supported by Program Insentif Riset Sistem Inovasi Nasional Gelombang Kedua Tahun Anggaran 2016, Kemenristekdikti. The authors would like to thank director of Satellite Technology Center (Pusteksat) LAPAN for providing research support facilities and to director of Space Technology Application Center for providing administration support.

## References

[1] Dong, X., Quegan, S., Yumiko, U., Hu, C., and Zeng, T., Feasibility Study of C- and L-band SAR Time Series Data in Tracking Indonesian Plantation and Natural Forest Cover Changes. *IEEE Journal of Selected Topics in Applied Earth Observations and Remote Sensing,* Vol. 8, No. 7, July 2015.

[2] Gambardella, A., Nunziata, F., and Migliaccio, M., A Physical Full-Resolution SAR Ship Detection Filter. *IEEE Geoscience and Remote Sensing Letters*, Vol. 5, No. 4, October 2008.

[3] Sumantyo, J. T. S., Shimada, M., Mathieu, Pierre-P., Abidin, H. Z., Long-Term Consecutive DInSAR for Volume Change Estimation of Land Deformation. *IEEE Transactions on Geoscience and Remote Sensing,* Vol. 50, No. 1, January 2012.

[4] Joyce, K. E., Belliss, S. E., Samsonov, S. V., McNeill, S. J., and Glassey, P. J., A review of the status of satellite remote sensing and image processing techniques for mapping natural

hazards and disasters. *Progress in Physical Geography*.

[5] Ivanov, A.Y. and Kucheiko, A.A., Distribution of oil spills in inland seas based on SAR image analysis: a comparison between the Black Sea and the Caspian Sea. *International Journal of Remote Sensing*, 37(9), pp.2101-2114.

[6] Kalogirou, V., Ferrazzoli, P., Della Vecchia, A. and Foumelis, M., On the SAR backscatter of burned forests: A model-based study in C-Band, over burned pine canopies. *IEEE Transactions on Geoscience and Remote Sensing*, 52(10), pp.6205-6215.

[7] Montomoli, F., Macelloni, G., Brogioni, M., Lemmetyinen, J., Cohen, J. and Rott, H., Observations and Simulation of Multifrequency SAR Data Over a Snow-Covered Boreal Forest. *IEEE Journal of Selected Topics in Applied Earth Observations and Remote Sensing*, 9(3), pp.1216-1228.

[8] Schmitt, M. and Zhu, X.X., Demonstration of Single-Pass Millimeterwave SAR Tomography for Forest Volumes. *IEEE Geoscience and Remote Sensing Letters*, 13(2), pp.202-206.

[9] Gou, S., Li, X. and Yang, X., Coastal Zone Classification With Fully Polarimetric SAR Imagery. *IEEE Geoscience and Remote Sensing Letters*, 13(11), pp.1616-1620.

[10] Hoang, H.K., Bernier, M., Duchesne, S. and Tran, Y.M., Rice Mapping Using RADARSAT-2 Dual-and Quad-Pol Data in a Complex Land-Use Watershed: Cau River Basin (Vietnam). *IEEE Journal of Selected Topics in Applied Earth Observations and Remote Sensing*, 9(7), pp.3082-3096.

[11] Erten, E., Lopez-Sanchez, J.M., Yuzugullu, O. and Hajnsek, I., Retrieval of agricultural crop height from space: A comparison of SAR techniques. *Remote Sensing of Environment*, 187, pp.130-144.

[12] Fang, L., Xu, Y., Yao, W. and Stilla, U., Estimation of glacier surface motion by robust phase correlation and point like features of SAR intensity images. *ISPRS Journal of Photogrammetry and Remote Sensing*, 121, pp.92-112.

[13] Fors, A.S., Brekke, C., Gerland, S., Doulgeris, A.P. and Beckers, J.F., Late Summer Arctic Sea Ice Surface Roughness Signatures in C-Band SAR Data. *IEEE Journal of Selected Topics in Applied Earth Observations and Remote Sensing*, *9*(3), pp.1199-1215.

[14] Giustarini, L., Hostache, R., Matgen, P., Schumann, G.J.P., Bates, P.D. and Mason, D.C., A change detection approach to flood mapping in urban areas using TerraSAR-X. *IEEE Transactions on Geoscience and Remote Sensing*, 51(4), pp.2417-2430.

[15] Ahmad, A., Classification simulation of RazakSAT satellite. *Procedia Engineering for Malaysian Technical Universities Conference on Engineering and Technology (MUCET) 2012*, vol. 53, pp. 472-482, 2013.

[16] Hasbi, W., and Karim, A., Lapan-A2 System Design For Equatorial Survaillance Missions. In *9th International Symposium of The International Academy of Astronautics (IAA) Berlin, April 2013.*

[17] Seah, P. H., Maverick Tan, T. C. and Meurer, R. H., TeLEOS-1 in multi-source maritime security and safety applications," *ACRS (Asian Conference on Remote Sensing),* Nay Pyi Taw, Myanmar, Oct. 27-31, 2014.

[18] http://www.agi.com/products/stk/modules/default.aspx/id/stk-pro

[19] Mattar K E. Modelling of the TerraSAR-X sensor modes in CSIAPS. *Technical Memorandum of DDRC Ottawa TM 2008-284.* Defence R & D Canada-Ottawa, 2009.

[20] Jie, C., Yin-qing, Z., and Chun-sheng, Li., Spaceborne synthetic aperture radar raw data simulation of three dimensional natural terrain. *Proceedings of 2001 CIE International Conference on Radar*. IEEE, 2001.

[21] Toth, C. and Jozkow, G., Remote sensing platform and sensors: A survey. *ISPRS Journal of Photogrammetry and Remote Sensing,* Vol. 115, pp. 22-36, 2016.

[22] Campbell, J. B., *Introduction to Remote Sensing, 4th Ed*. The Guilford Press, 2007.